ACS OMEGA

http://pubs.acs.org/journal/acsodf Article

Minimum CO_2 Miscibility Pressure Evaluation using Interfacial Tension (IFT) and Slim-tube Hybrid Tests

Muslim Abdurrahman,* Asep Kurnia Permadi, Agus Arsad, Anis Farhana Abdul Rahman,* Wisup Bae, Ully Zakyatul Husna, Ai Ling Pang, and Rifal Fauzi

Cite This: *ACS Omega* 2023, 8, 8703−8711 Read Online

ABSTRACT: The effectiveness of CO_2-enhanced oil recovery (EOR) is strongly dependent on the CO_2−oil minimum miscible pressure (MMP) value, which can be estimated using various methods. In this study, interfacial tension (IFT) and slim-tube tests were used to estimate the MMP value. Experimental results indicated that the IFT test had a higher MMP value than the slim-tube test. Particularly, the outcomes of IFT and the slim-tube tests differed slightly, i.e., 0.7% and 4.3% at 60 and 66 °C, respectively. Furthermore, the current work also compares MMP data gathered using visual observation and equation of state (EOS) simulation. The MMP estimated by EOS is higher but close to the IFT and slim-tube recovery factor method, where all results are within the 1650−1700 psi and 1700−1800 psi visual observation ranges at 60 and 66 °C, respectively. However, MMP deviations concerning the slim-tube test and EOS were consistent at different temperatures. This study offers an alternative to estimate and evaluate CO_2−oil MMP for EOR applications accurately and efficiently.

1. INTRODUCTION

CO_2 gas injection is one of the most renowned EOR methods because it improves oil recovery while lowering greenhouse gas emissions.[1] Aside from being a cost-effective method, CO_2 injection may recover more oil at above-minimum miscible pressure (MMP) conditions due to the miscibility of CO_2 and the content of the oil reservoir. Oil swelling at MMP lowered IFT and viscosity between the injected CO_2 and the oil. Pure CO_2 is a colorless and odorless gas that is 1.67 times heavier than air under standard conditions. Above critical temperature (31.0 °C), CO_2 behaves as a gas, and as supercritical pressures increase (above 1070 psi), it behaves more like a liquid. In addition, in the supercritical situation, CO_2 density is close to oil density; hence, it is readily miscible with reservoir fluid. Moreover, before injection, CO_2 had to be separated from possible Indonesian oil (West Java) or gas/coal bed methane (Natuna, Muara Bulian). It was achieved using several approaches such as the new membrane process in Kadirpur, Pakistan, the expensive single/multistage cryogenic process, or the rectisol process, which is a cheaper monoethanol-amine (MEA) chemical absorption process similar to that in Weyburn, Canada.[2−4]

Furthermore, MMP is typically determined through laboratory tests, simulations, or correlations presented in the literature. Several researchers, such as Yellig and Metcalfe,[5] Yu et al.,[6] Zheng et al.,[7] Ahmad et al.[8] and Zhao et al.[9] have attempted to measure MMP experimentally. In addition, other studies have measured MMP in different ways, like the simulations by Ahmed[10] or correlation and machine learning by Chen et al.,[11] Soori et al.,[12] and Chen et al.[13] Recently, other researchers predicted MMP by conducting IFT tests or slim-tube tests.[14−18]

IFT is the free energy per unit surface area of the interface between two phases. It is possible to resolve this using the Laplace capillary equation as in the work of Firoozabadi.[19] Despite the existence of various methods to resolve IFT, the pendant-drop method has been considered the most capable of measuring IFT at high temperature and pressure. In a previous study, the pendant-drop method was considered by Saad et al.[20] to calculate IFT.

Practically, the method requires accurate information regarding the density change between the two fluids. This method may be the most preferred due to its considerably tiny contact interface between solid substrates, which is observed using the tip cross-section of a needle. Unfortunately, the method strongly depends on drop profile determination precision. Drop profile may lead to significant errors in the

Received: December 20, 2022
Accepted: February 14, 2023
Published: February 24, 2023

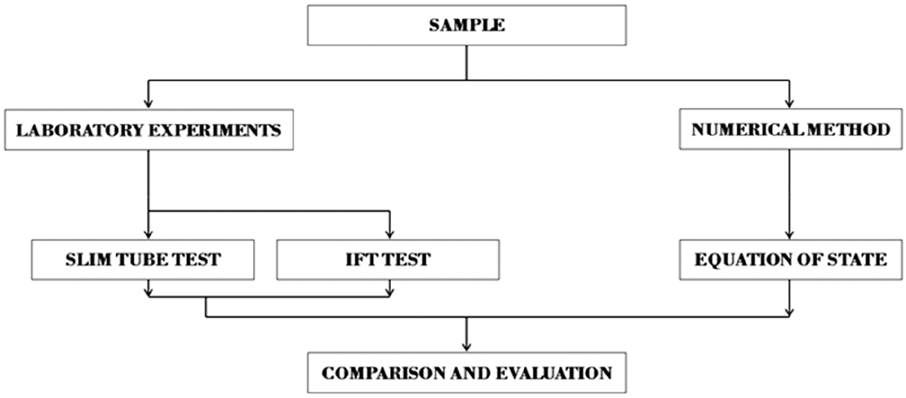

Figure 1. Flow of research methodology.

IFT value, which is considered a limitation of the present method. Moreover, the drop profile aspect ratio can lead to an inaccurate IFT determination.

However, the slim-tube test is sometimes regarded as an industry standard, despite the fact that it is only a one-dimensional sand-packed reservoir model. To simulate the liquid−gas fluid flow in porous media, it is typically saturated with reservoir oil and injected with CO_2 at various temperatures, injection rates, and pressures. The produced effluent is then collected in the buret. The recovery factor (RF) increases with pressure until a break-over point is reached, as depicted in Figure 6, where the curve slope changes at about 90% RF.[17] The MMP from this test aligns well with the simulation if very accurate reservoir data are taken.[6,11,13,14,21] Yet, a combination of IFT and slim-tube methods has rarely been used to estimate MMP. Thus, this study was conducted to minimize the uncertainties by comparing MMP results from both techniques.

Jessen and Orr[22] estimated MMP through visual observations. The experiments successfully visually observed three different stages during the CO_2 oil mixing procedure, which is extraction, extraction−condensation, and condensation. The study specifically proposed that MMP can be estimated when a CO_2-rich phase and CO_2 vapor interface disappear. In another study, MMP was predicted by visual observation during the slim-tube test by Abdurrahman et al.[17] MMP occurs when the oil is brighter than it was initially. This phenomenon occurs practically after the slope with a high recovery factor change to a smaller one. Visual observation is a quick technique to estimate MMP under a high-pressure visual cell. However, this method has been considered inaccurate. It is recommended as a supplementary method to estimate MMP.

To this extent, no previous research has been included such extensive evaluations concerning simultaneous techniques combining the IFT, slim-tube, simulation, and visual observation tests to evaluate miscibility. A previous study[23] reported using different miscibility evaluation techniques such as the IFT and slim-tube tests, raising bubble apparatus, and pressure−composition diagram. Yang and Gu[16] utilized the combination of the IFT test and raising bubble apparatus to estimate MMP. Nobakht et al.[14] compared MMP results using simulation and the IFT test. Meanwhile, Hemmati-Sarapardeh et al.[15] and Yang et al.[24] only estimated MMP through IFT experiments.

However, these researchers did not compare MMP results from their IFT tests with other tests in the same graph, such as the slim-tube and simulation tests; they just compared MMP results. In the current study, a new technique is proposed by exploring the combination of these works to develop a merit method for estimating MMP. First, the IFT vs pressure and slim-tube test vs pressure results are plotted in the same figure, which has never been used extensively in previous research. This graph makes it easy to clarify MMP discrepancies concerning both methods. Thus, it is advantageous to use this technique. It also proves that the slim-tube test is an appropriate method to estimate MMP, as suggested by Abdurrahman et al.[17,25,26] Second, the MMP is determined through simulation using the equation of state (EOS). Third, visual observation is conducted using photos or videos, as previously done by Jessen and Orr[22] and Abdurrahman et al.[17,25,26] In the current case, the shape of the oil drop is observed until it disappears in the display cell. However, the method may be inaccurate. So, this study only takes it as a supplementary method to estimate MMP. The results are compared to investigate discrepancies between the resulting MMPs to reduce uncertainties.

This study aims to provide an enhanced approach for estimating and evaluating MMP. As explained previously, the measurement and computation are proposed by comprehensively considering existing methods. The slim-tube method is a proper way to estimate MMP and is considered an industry standard, although this method is a one-dimensional sand-packed reservoir model. Meanwhile, the visual observation method is fast but prone to inaccuracies. The IFT test is suitable for critical conditions, but this method strongly depends on the drop profile precision.

On the other hand, MMP EOS simulation has been recognized as an easy and quick method to calculate MMP. These methods have been developed to enable a quick and cost-effective way of predicting the minimum miscibility pressure. There are at least three advantages to applying these techniques. First, the slim-tube test may be an appropriate method for estimating MMP. Second, it may require less time and fluid sample consumption. Third, these methods can be conducted simultaneously to minimize any uncertainty in estimating MMP. This method efficiently provides more accurate CO_2−oil MMP evaluation results.

In a nutshell, the results of this study will later contribute to the practice of testing MMP, especially for the analysis of the effectiveness of CO_2-enhanced oil recovery (EOR). The new method used in this study which combines IFT, slim-tube, simulation, and visual observation tests to evaluate miscibility has never been found in previous works. This study is a new development in creating a suitable method for estimating

https://doi.org/10.1021/acsomega.2c08085
ACS Omega 2023, 8, 8703−8711

MMP. The combined method used should have a higher level of reliability due to the minimum uncertainties and more accuracy.

2. PREPARATION AND METHODOLOGY

To produce satisfactory results for the slim-tube test, IFT test, visual observation, or simulation, multiple steps are intentionally implemented. The overall results are then compared to investigate discrepancies. Figure 1 depicts the complete flow of the research methodology. Each stage of the present study is described in the following explanations.

2.1. Materials. The experiment utilizes 99.9% pure CO_2 gas. Crude oil was first extracted from a reservoir at the Air Benakat Formation in Indonesia's Jambi province. The oil properties and composition are shown in Tables 1 and 2. The density of CO_2 was calculated using the NIST program at different pressures and temperatures. The current work states that the oil density is constant (0.823 gr/cc). According to Wang et al.,[27] the variations in oil density caused by CO_2 dissolution at high pressure are minor.

Table 1. Sample Properties

properties	AB-5
API gravity	41.38
reservoir temperature (T_r) [°F]	150
reservoir pressure (p_r) [psi]	1134
bubble point pressure (p_b) [psi]	1116
viscosity [cp]	0.21

Table 2. Oil Composition

component	symbol	mole [%]	weight [%]
hydrogen sulfide	H_2S	0.00	0.00
carbon dioxide	CO_2	0.12	0.05
nitrogen	N_2	0.65	0.17
methane	C_1	18.50	2.71
ethane	C_2	1.79	0.59
propane	C_3	1.87	0.75
iso-butane	i-C_4	0.84	0.45
n-butane	n-C_4	1.37	0.73
iso-pentane	i-C_5	1.64	1.08
n-pentane	n-C_5	0.99	0.65
hexanes	C_6	2.58	2.03
heptane plus	C_{7+}	69.65	90.89
total		100.00	100.00
properties of heptane plus:			
specific gravity @ 60/60 °F		0.8308	
molecular weight		142.73	

2.2. Experimental Apparatus and Procedures. *2.2.1. IFT Test.* Figure 2 depicts the experimental diagram for the IFT test. Other equipment includes two syringe pumps for water, a CO_2 injection pump (ISCO Company), a goniometer apparatus (Ramé-Hart Surface Science Instruments), and a visual cell. High-pressure and high-temperature visual cells are suitable for measuring the IFT in a reservoir. The cells have a 30 mm diameter, 60 mm height, and 16 mm thickness. The maximum operating temperature and pressure of the visual cells are 300 °C and 3000 psi, respectively. The stainless-steel needle has an outer diameter of 0.91 mm and a length of 50 mm. In addition, a couple of sapphire glasses are positioned next to each other and fitted inside the visual cells. The glass window is 10-mm-thick and 30 mm in diameter. Next, a specific amount of dead oil is added into the piston chamber, which has a maximum operating pressure of 3000 psi. Simultaneously, a check valve and a meter are installed to maintain a steady oil flow rate and to prevent cell flow-back. Technically, the temperature inside the cell is monitored using a calibrated thermocouple. Furthermore, a pressure gauge is used to measure the system pressure. Then, all apparatuses are fitted through stainless steel tubing lines.

Prior to the measurement stages, all apparatuses and lines must be appropriately cleaned using toluene, followed by drying with nitrogen and vacuuming. Furthermore, the pressure within the cell should be chemically controlled by injecting CO_2. In addition, a constant temperature should be maintained using a heater. Next, sequential experiments were run at different pressures (700 to 2500 psi) and temperatures (60 to 66 °C). Once the cell pressure and temperature are maintained at constant levels according to the desired setting (20−30 min), water is pumped into the chamber at 0.1 cc/min.

Simultaneously, the piston forces the dead oil up into the chamber. Next, the dead oil flows from the chamber over a tube line to the needle's tip, where it suspends. The oil drop should be kept stable for a specific period by adjusting the metering valve. For this testing, the oil drop should be kept stable for 40 to 60 s (s). This range is adopted because it has been suggested by previous researchers.[16,24]

Furthermore, IFT measurement is carried out based on the geometrical assessment of the drop image as taken by the camera. In order for a drop image to be considered excellent and representative, the oil and CO_2 phases must be clearly separated, which should be appropriately achieved for the IFT value to be accurate. Thus, adjusting the camera focus and light intensity is critical to obtaining a good image setting. A monitor and computer were used to connect the camera system to an image capture board and image analysis software, including DROP-image, which determines IFT. To improve IFT certainty, the measurement was repeated three times.

After the measurement was complete, the lines and apparatus were cleaned again using toluene, followed by nitrogen-based drying and vacuuming. As a function of temperature, MMP can be calculated theoretically by extrapolating IFT's linear trend line.

2.2.2. Slim-Tube Test. The slim-tube test employs a long-coiled tube packed with a specific mesh size of sand. The solvent (CO_2) was injected at a specific temperature into the oil-saturated tube at several test pressures. Oil recovery was then measured as a function of pressure. The estimated MMP of the oil−solvent system is represented by the intersection between the two trend lines in the graph. The experiment conducted in the current study refers to two prior studies, i.e., Abdurrahman et al.[17] and Adel et al.[18]

Figure 3 depicts the slim-tube test experiment diagram. The system involves of a high-pressure cell with a 12 mm diameter, 80 mm height, 16 mm thickness, and a sapphire-based material. The cell was installed in an air bath system with a heater to keep the temperature stable. A cooler equipped with a precision ISCO pump was utilized to inject CO_2. The cooler was used to maintain the liquid state of CO_2 before it was injected into the cell. Additionally, a stirring bar was placed at the bottom of the cell to mix oil and CO_2 until an equilibrium was reached. The specifications of the slim tube are provided in Table 3.

https://doi.org/10.1021/acsomega.2c08085
ACS Omega 2023, 8, 8703−8711

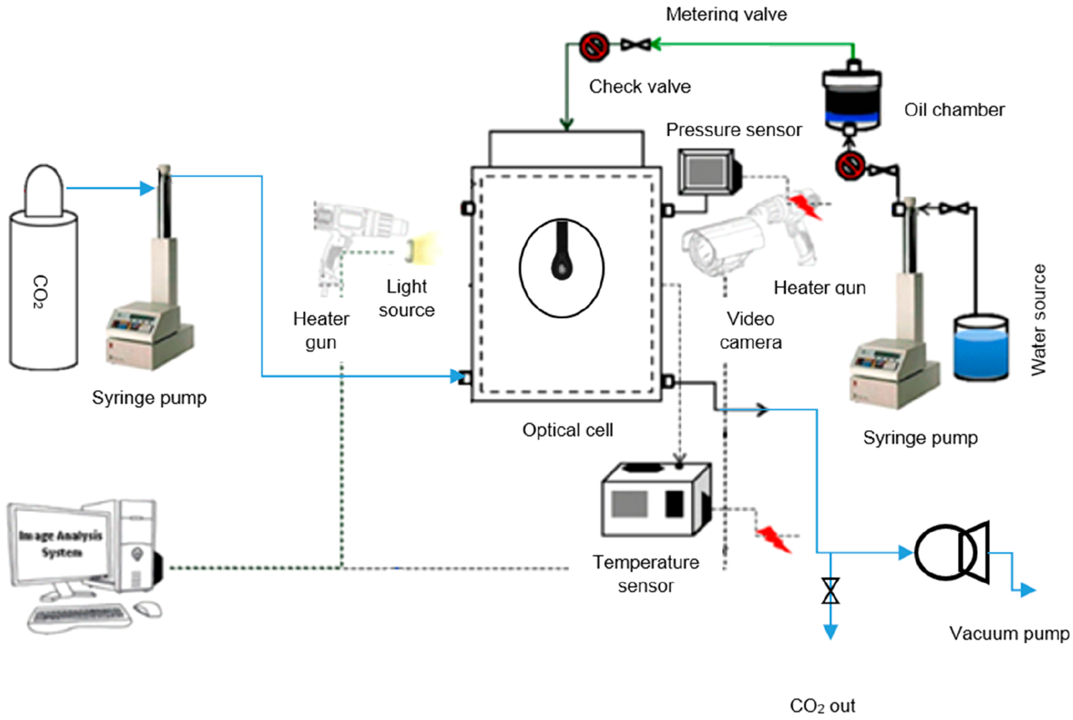

Figure 2. IFT experimental diagram.[26]

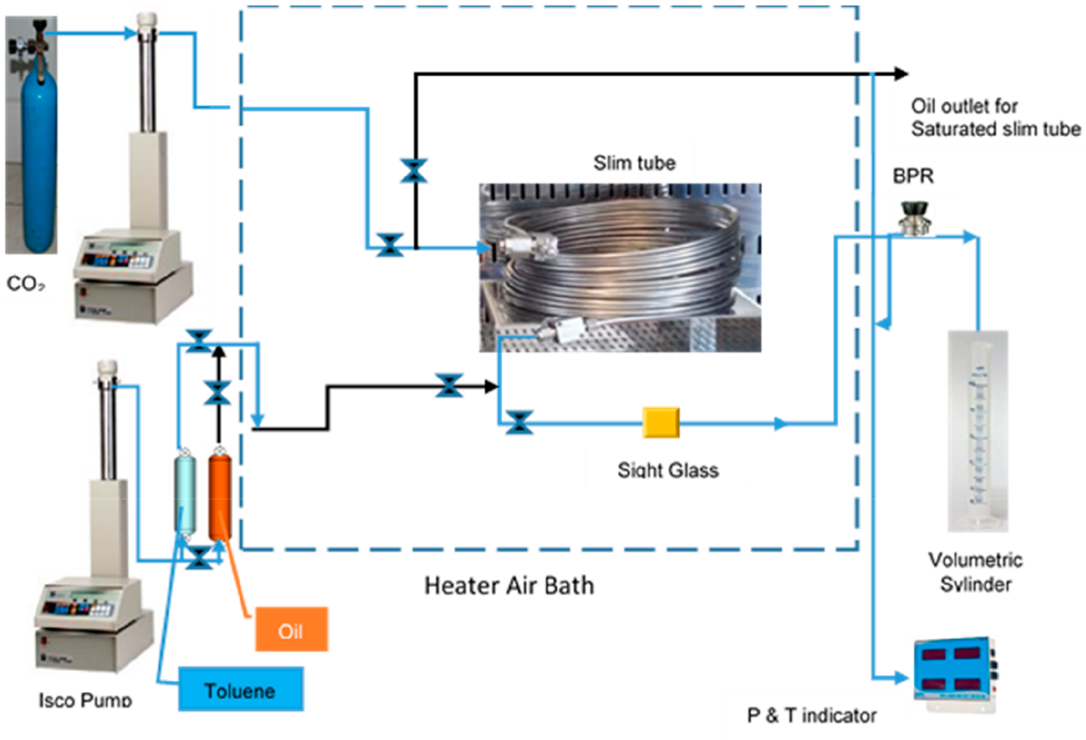

Figure 3. Slim tube test experimental diagram.[26]

Before starting the measurement, the cell was thoroughly washed with toluene and dried with nitrogen. The cell was then filled with a 2.7 cm^3 filtered crude oil sample, or about 30% of the total volume under room conditions, as suggested by Alhosani et al.[28] The current experiment used the same temperature as the IFT experiment by injecting CO_2 gas into the cell at a specific pressure level. Next, the pressure was gradually increased by 200 psi until it reached 2400 psi. In parallel, the stir bar inside the cell was rotated continuously to allow a CO_2−crude oil mixture equilibrium. According to Adel et al.,[18] data point selection should be based on linear trends instead of the transitional zone to prevent MMP deviation.

2.3. EOS Simulation. A simulation was recognized as a quick and easy method to calculate MMP and eliminate doubts about experimental results. The simulation results were posted in the current study to endorse the actual experimental results.

https://doi.org/10.1021/acsomega.2c08085
ACS Omega 2023, 8, 8703−8711

Table 3. Slim Tube Specifications

column material	316 stainless steels
internal diameter, in	0.18
length, ft	40.78
packing material	Hama Sand #8
porosity, %	35
permeability, Darcy	0.70

Furthermore, a cell-to-cell approach was used to detect the pressure at which a critical point was reached in the tie line in order to estimate any miscible conditions. Simulation methods are faster than experiments because they require gas injection composition, oil composition, and reservoir temperature data (in this case: 60 and 66 °C).

3. RESULTS

3.1. Estimation of MMP via IFT. According to Yang and Gu,[16] light and moderate components extracted quickly from the oil drop may have caused CO_2 to produce rich oil due to diffusion. The phenomenon reduced IFT between oil and CO_2. However, when the pressure rises and approaches the miscibility level, heavy components remain in the crude oil. As a result, the oil drop starts to shrink and the IFT decreases at a slower rate. Based on Yang and Gu's explanation, the two regions concerning the IFT test in this study are intentionally referred to as two identifications, which are region A (diffusion stage) and region B (shrinkage stage). Lashkarbolooki et al. calculated MMP using linear extrapolation on a diffusion line versus pressure data to a zero IFT (horizontal axis) called the vanishing interfacial tension (VIT).[29] The linear regression for estimating MMP at 60 and 66 °C temperature settings are expressed using eqs 1 and 2:

$$\mathrm{IFT} = -0.0262 \times \mathrm{Pressure} + 42.22 \quad (1)$$

$$\mathrm{IFT} = -0.0226 \times \mathrm{Pressure} + 40.17 \quad (2)$$

The first and second equations were used to estimate MMP at 60 and 66 °C with correlation coefficients (R^2) of 99.9%. The MMP determined using the current method was acceptable, as determined using the R^2 value concerning the two equations. However, the equations are applicable for pressure ranges between 700 psi and 1500 psi at 60 and 66 °C. The equations are not applicable beyond these levels due to a different phenomenon.

The MMPs were estimated under elevated pressure and temperature, as presented in Figures 4 and 5. At zero IFT, eqs 1 and 2 indicate that IFT shows miscibility at 1624 and 1760 psi for 60 and 66 °C. Meanwhile, MMP rises as the temperature of the system rises. The incremental MMP rise could be caused by a temperature increase from 60 to 66 °C, resulting in a pressure increase of 166 psi. Hence, the increase is about 27.7 psi/°C. These findings are consistent with an earlier study by Sarapardeh et al.,[15] where an MMP increase occurred at about 22.6 psi/°C. Higher temperatures reduce CO_2 solubility in crude oil, leading to higher MMP. Furthermore, IFT vs pressure slope is slightly different. As temperature increases, the IFT vs pressure slope rises, leading to a higher MMP. Figure 5 shows a greater IFT slope (m) at −0.023 than that in Figure 4 (−0.026). These figures indicate that the slope increases with temperature. Hence, a higher slope causes a higher MMP.

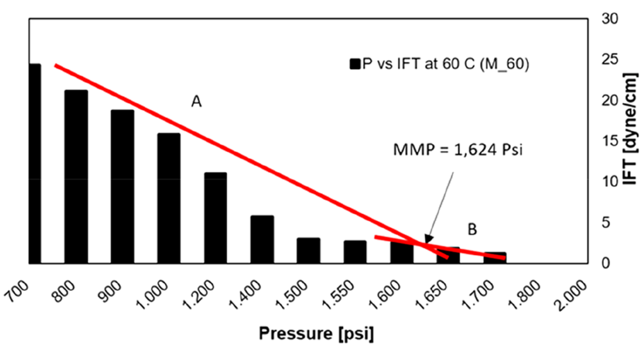

Figure 4. MMP from IFT test at T = 60 °C.

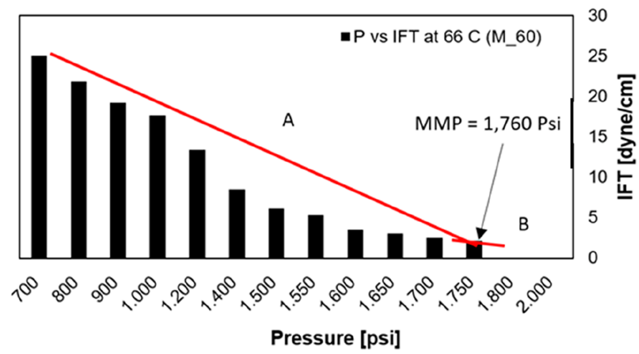

Figure 5. MMP from IFT test at T = 66 °C.

3.2. Estimation of MMP Using Recovery Factor. This method estimated MMP by visually analyzing plots of the recovery factor vs pressure. Practically, the MMP was determined at the intersection of the slope lines, as shown in Figure 6. CO_2 injection into the cell at 60 °C initiated condensation where CO_2 begins to diffuse into the crude oil. Based on the figure, the intersection between the trend lines occurs at 1540 psi. Consequently, the MMP was ascertained as 1540 psi for a 60 °C temperature setting. As shown in Figure 7, the same method was employed for the other temperature settings, where MMP was discovered at 1700 psi.

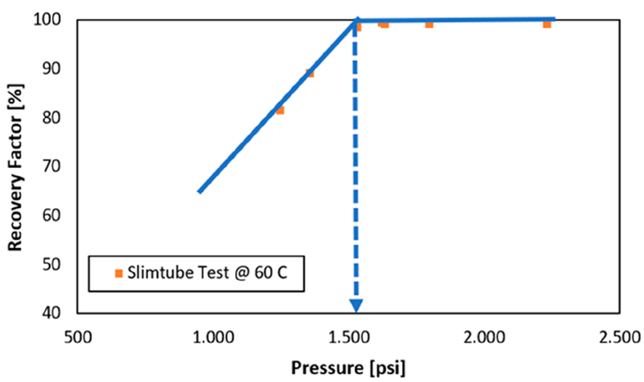

Figure 6. MMP from the slim-tube tests at T = 60 °C.

In the current study, every 6 °C increase in temperature leads to a 100 psi MMP increase, as presented in Figures 6 and 7. In other words, it indicates a ratio of 16.7 psi/°C. This phenomenon is similar to the previous work by Zhang and co-workers.[23] In their study, a temperature-specific pressure increase was between 18.10 psi/°C and 27.02 psi/°C.

3.3. Estimation of MMP via Visual Observations during IFT Test. The current study applied the visual

https://doi.org/10.1021/acsomega.2c08085
ACS Omega 2023, 8, 8703−8711

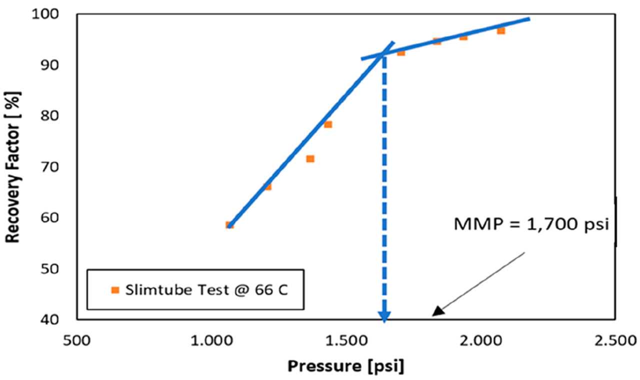

Figure 7. MMP from the slim-tube tests at T = 66 °C.

observation method to predict MMP. Dong et al.[4] recommended that MMP could be determined using visual observation during a slim-tube test experiment. This method was also proven by Abdurrahman et al.[17] to predict MMP. The IFT test process used for this study is depicted in Figures 8 and 9. As the pressure rises, the oil drop changes slightly. Oil drop shape changes irregularly between 1650 and 1700 psi and 1700 and 1800 psi for 60 and 66 °C temperature settings, respectively. As the oil disappears from the needle tip, a miscible phenomenon occurs between oil and CO_2 for every temperature setting. When the oil drop changes to an irregular shape, the software may not be able to calculate IFT. In such a situation, the system estimates a value near MMP.

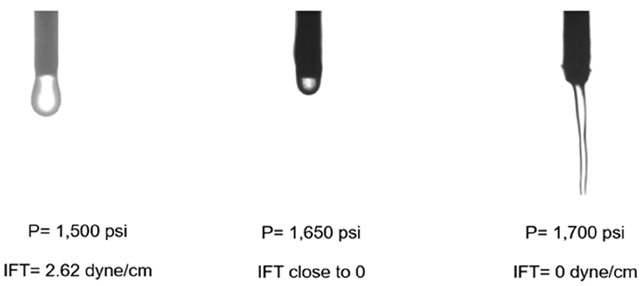

Figure 8. MMP by visual observation under IFT test at T = 60 °C.[26]

Figure 9. MMP by visual observation under IFT test at T = 66 °C.[26]

3.4. Estimation of MMP via EOS Simulations. The MMP calculation in the current study was conducted without any tuning to predict the phase behavior data, which has also been well suggested by a previous study.[30,31] According to simulation results based on an EOS (Peng−Robinson), the MMP for the corresponding temperatures is 1785 psi and 1675 psi. Table 4 displays the key parameters of hydrocarbon and nonhydrocarbon components, which are processed as recommended by the WinProp-CMG software. The details of binary interaction coefficients are comprehensively provided in Table 5.

Table 4. Critical Properties of the Components

component	critical pressure [atm]	critical temperature [K]	acentric factor	mole weight
H_2S	88.2	373.2	0.100	34.08
CO_2	72.8	304.2	0.225	44.01
N_2	33.5	126.2	0.040	28.01
CH_4	45.4	190.6	0.008	16.04
C_2H_6	48.2	305.4	0.098	30.07
C_3H_8	41.9	369.8	0.152	44.09
IC_4	36.0	408.1	0.176	58.12
NC_4	37.5	425.2	0.193	58.12
IC_5	33.4	460.4	0.227	72.15
NC_5	33.3	469.6	0.251	72.15
FC_6	32.5	507.5	0.275	86.00
C_{7+}	25.3	663.9	0.401	142.73

4. DISCUSSION

4.1. Comparing MMP Estimations between IFT and Recovery Factor. CO_2 diffuses into crude oil within the diffusion region (region A), as shown in Figures 4 and 5, resulting in oil swelling and a rapidly reducing IFT. A decrease of 24.5 to 2.93 dyn/cm was observed in region A of the study at 60 °C, while a decrease of 24.9 to 3.4 dyn/cm was observed at 66 °C. However, medium components are scarce, leaving only heavy components as the pressure maintains the increment in the oil drop. Conversely, the heavy components of crude oil in region B (shrinkage region) maintain their impact on the reduction of IFT. In region B, the IFT changed from 2.6 to 2.5 dyn/cm at 60 °C and 3.0 to 2.1 dyn/cm at 66 °C. In the case of miscibility, molecular effects can be explained as follows: a rise in CO_2 injection pressure causes more CO_2 molecules to diffuse into oil drops, resulting in a rapid loss of density. A higher injection pressure can cause the CO_2 to become denser, thereby minimizing the difference in density between the oil drop and CO_2. A lower density difference indicates that CO_2 and oil behave closely in region B due to intermolecular forces. Specifically, when the intermolecular forces between CO_2 and crude oil are balanced, the interface between these two phases may disappear.

Furthermore, a near miscibility condition is proposed at the intersection of regions A and B of the IFT vs pressure plot. The IFT decreases rapidly as the pressure increases before the miscibility region is reached. Similarly, the IFT above the region of near miscibility, or the so-called shrinkage region, slowly decreases with a pressure increase due to the dominance of heavy components in crude oil. Moreover, the intersection between linear trend lines is vital to determining the MMP through a slim-tube test. During analysis, data points in the transition region should be avoided. The region after the transition zone cannot be seen during the IFT test because the IFT values are too small and require more accurate equipment. The break-over line during the slim-tube and IFT test experiments shows a similar value.

Figures 10 and 11 exhibit combined plots concerning the IFT and slim-tube tests at 60 and 66 °C, respectively. Clearly, the MMP corresponding to the slim-tube test aligns well with the IFT test. According to the results obtained from the slim-

https://doi.org/10.1021/acsomega.2c08085
ACS Omega 2023, 8, 8703−8711

Table 5. Binary Interaction Coefficients

component	H_2S	CO_2	N_2	CH_4(HC)	C_2H_6(HC)	C_3H_8(HC)	IC_4(HC)	NC_4(HC)	IC_5(HC)	NC_5(HC)	FC_6(HC)	C_{7+}(HC)
H_2S	zero	9.60×10^{-02}	1.76×10^{-01}	8.00×10^{-02}	7.00×10^{-02}	7.00×10^{-02}	6.00×10^{-02}	6.00×10^{-02}	6.00×10^{-02}	6.00×10^{-02}	0.00×10^{00}	0.00×10^{00}
CO_2	9.60×10^{-02}	zero	-2.00×10^{-02}	1.03×10^{-01}	1.30×10^{-01}	1.35×10^{-01}	1.30×10^{-01}	1.30×10^{-01}	1.25×10^{-01}	1.25×10^{-01}	1.50×10^{-01}	0.00×10^{00}
N_2	1.76×10^{-01}	-2.00×10^{-02}	zero	3.10×10^{-02}	4.20×10^{-02}	9.10×10^{-02}	9.50×10^{-02}	9.50×10^{-02}	9.50×10^{-02}	9.50×10^{-02}	1.20×10^{-01}	0.00×10^{00}
CH_4(HC)	8.00×10^{-02}	1.03×10^{-01}	3.10×10^{-02}	zero	2.69×10^{-03}	8.54×10^{-03}	1.57×10^{-02}	1.47×10^{-02}	2.09×10^{-02}	2.06×10^{-02}	2.53×10^{-02}	4.66×10^{-02}
C_2H_6(HC)	7.00×10^{-02}	1.30×10^{-01}	4.20×10^{-02}	2.69×10^{-03}	zero	1.66×10^{-03}	5.49×10^{-03}	4.91×10^{-03}	8.73×10^{-03}	8.58×10^{-03}	1.17×10^{-02}	2.76×10^{-02}
C_3H_8(HC)	7.00×10^{-02}	1.35×10^{-01}	9.10×10^{-02}	8.54×10^{-03}	1.66×10^{-03}	zero	1.12×10^{-03}	8.66×10^{-04}	2.80×10^{-03}	2.71×10^{-03}	4.62×10^{-03}	1.60×10^{-02}
IC_4(HC)	6.00×10^{-02}	1.30×10^{-01}	9.50×10^{-02}	1.57×10^{-02}	5.49×10^{-03}	1.12×10^{-03}	zero	1.59×10^{-05}	3.82×10^{-04}	3.50×10^{-04}	1.20×10^{-03}	8.72×10^{-03}
NC_4(HC)	6.00×10^{-02}	1.30×10^{-01}	9.50×10^{-02}	1.47×10^{-02}	4.91×10^{-03}	8.66×10^{-04}	1.59×10^{-05}	zero	5.54×10^{-04}	5.15×10^{-04}	1.49×10^{-03}	9.48×10^{-03}
IC_5(HC)	6.00×10^{-02}	1.25×10^{-01}	9.50×10^{-02}	2.09×10^{-02}	8.73×10^{-03}	2.80×10^{-03}	3.82×10^{-04}	5.54×10^{-04}	zero	7.17×10^{-07}	2.28×10^{-04}	5.48×10^{-03}
NC_5(HC)	6.00×10^{-02}	1.25×10^{-01}	9.50×10^{-02}	2.06×10^{-02}	8.58×10^{-03}	2.71×10^{-03}	3.50×10^{-04}	5.15×10^{-04}	7.17×10^{-07}	zero	2.55×10^{-04}	5.60×10^{-03}
FC_6(HC)	0.00×10^{00}	1.50×10^{-01}	1.20×10^{-01}	2.53×10^{-02}	1.17×10^{-02}	4.62×10^{-03}	1.20×10^{-03}	1.49×10^{-03}	2.28×10^{-04}	2.55×10^{-04}	zero	3.48×10^{-03}
C_{7+}(HC)	0.00×10^{00}	0.00×10^{00}	0.00×10^{00}	4.66×10^{-02}	2.76×10^{-02}	1.60×10^{-02}	8.72×10^{-03}	9.48×10^{-03}	5.48×10^{-03}	5.60×10^{-03}	3.48×10^{-03}	zero

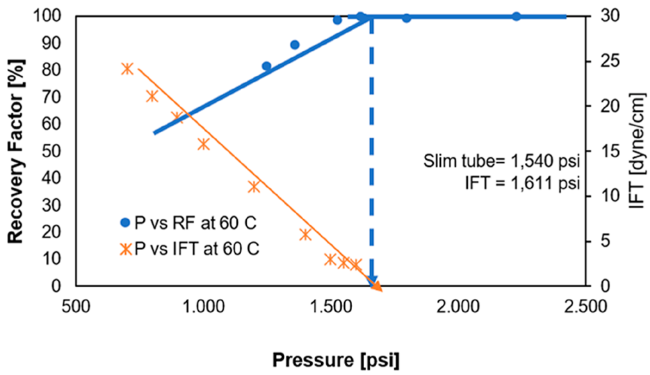

Figure 10. MMP from IFT (circle) and slim-tube (x) tests at T = 60 °C.

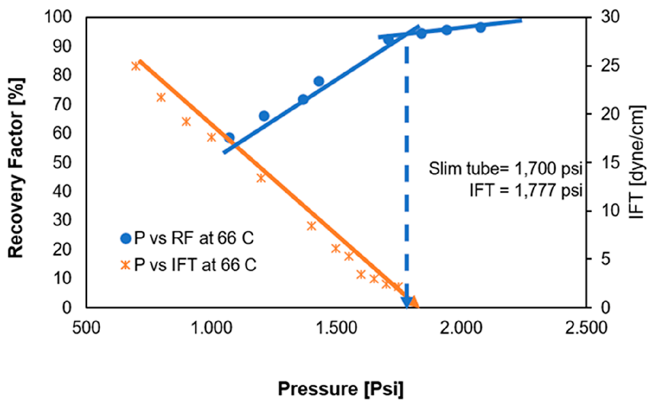

Figure 11. MMP from IFT (circle) and slim-tube (x) tests at T = 66 °C

tube and IFT tests, MMP values were satisfactory. Table 6 shows the percentage difference between the results of the

Table 6. MMP Differences among the Results

methods	MMP, psi 60 °C	MMP, psi 66 °C	MMP deviation to IFT,[a] % 60 °C	MMP deviation to IFT,[a] % 66 °C
slim-tube test	1540	1700	5.4	3.5
EOS	1675	1785	−3.0	−1.4
IFT	1624	1760		

[a]The difference is calculated as (IFT − slim tube)/(slim tube) or (IFT − EOS)/EOS.

slim-tube and IFT tests. The differences are about 0.7% and 4.3% for 60 and 66 °C temperatures, respectively. The MMP data obtained from the IFT test are higher at lower temperatures than the slim-tube test. However, it falls within a reasonable range at a higher temperature because the results exhibit only a minor discrepancy.

4.2. Comparison of MMP Estimations between Experiments vs Simulation. Oil samples may have caused a slight discrepancy between the results of the discussed methods, as the IFT and slim-tube test experiments used dead oil whereas the simulation used live oil. MMP has been slightly higher due to different gas constitutions concerning methane and nitrogen. Table 6 shows that the results of the slim-tube test and simulation differ by about 4.5% and 4.8% at 60 and 66 °C, respectively. Meanwhile, the outcomes of the IFT test and

https://doi.org/10.1021/acsomega.2c08085
ACS Omega 2023, 8, 8703−8711

the simulation differ by 3.8% and 0.4% for 60 and 66 °C, respectively.

The slim-tube and IFT tests have provided reasonable MMP estimates. According to the table, MMP estimated by the IFT method is slightly closer to the EOS method than the slim-tube recovery factor method. However, the deviations of MMP attained from the slim-tube test to EOS were consistent at different temperatures. According to the table, using different methods during experiments may have resulted in different results, even though the discrepancy is small. MMP data obtained from EOS were generally higher than IFT and slim-tube tests.

4.3. Comparison of MMP Estimations by IFT and Slim Tube Tests vs Visual Observation. MMP estimation by visual observation is a distinguished advantage of an IFT experiment. It can be performed by monitoring videos or pictures captured during an IFT experiment. The pressure data obtained from the method include an MMP range. It is not possible to estimate the exact MMP value. Oil is practically miscible when it disappears from the tip of the needle. The method is considerably robust, while the results require a further comparison to other methods to yield consistent results. Figures 8 and 9 exhibit the range of MMP for each temperature. Roughly, miscibility is proven as IFT decreases. The miscibility occurs at 1700 and 1800 psi for 60 and 66 °C temperatures, respectively. The last image in these figures displays miscible conditions due to the absence of an interface between oil and gas. In addition, miscibility pressure determined by visual observation is higher than MMP data obtained from the IFT vs pressure plot, where there are discrepancies among the results at about 5.5% and 1.3% at 60 and 66 °C temperatures, respectively.

Furthermore, the current work compares MMP data obtained from visual observation during the IFT test with those acquired from the slim-tube test. The visually observed MMP range is between 1500 psi and 1700 psi at 60 °C. In another observation, the MMP range data fall between 1700 psi and 1800 psi at 66 °C. The MMP by visual observation is higher than that obtained by the recovery factor vs pressure plot, indicating discrepancies between 6.25% and 5.9% at 60 and 66 °C, respectively. The pendant drop-shaped moving boundary interface was detected between the fluids; therefore, the changing volumes of oil or CO_2 solubility in oil were observed. It is evident from these observations that the range of MMP data is greater than that of IFT and slim-tube tests. However, information gathered through visual observations is noteworthy because it offers additional information about the MMP range during IFT experiments. Figures 8 and 9 have perfectly shown miscibility, but miscibility pressure is not at the minimum feasible level. Instead of a range of values, the visual observation could be closer to those of IFT and slim-tube tests if the acoustic pulse-echo (APE) method was used to calculate oil volume expansion factors.[31]

5. CONCLUSIONS

The following conclusions emerge based on the findings and facts originating from this research:

1. The current study used a sample of 41.38 API crude oil obtained from the Air Benakat Formation, in which the MMP resulting from the IFT test aligns well with the slim-tube test and the simulation.

2. The simultaneous plot helps act as a suitable technique for investigating any discrepancy between MMP values attained from the IFT and slim-tube tests.

3. The MMP data obtained from IFT were higher than those of the slim-tube test at lower temperatures. Nevertheless, the discrepancies between these results were within an acceptable range at a higher temperature.

4. Visual observation during an IFT test can be used to recognize the miscibility phenomenon. The method was found to be robust but may produce a slightly higher MMP than the IFT and slim-tube tests.

5. This study provides an advancement in terms of analysis on the effectiveness of CO_2-enhanced oil recovery (EOR) by applying a combined method which never had been used previously. This method can be considered one of the standards in estimating MMP because the uncertainty is much smaller and produces higher accuracy.

AUTHOR INFORMATION

Corresponding Authors

Muslim Abdurrahman − *Department of Petroleum Engineering, Universitas Islam Riau, Riau 28284, Indonesia;* orcid.org/0000-0003-0584-861X; Email: muslim@eng.uir.ac.id

Anis Farhana Abdul Rahman − *UTM-MPRC Institute for Oil and Gas, Faculty of Chemical and Energy Engineering, Universiti Teknologi Malaysia, 81310 Skudai, Malaysia;* Email: afarhana91@gmail.com

Authors

Asep Kurnia Permadi − *Department of Petroleum Engineering, Institut Teknologi Bandung, Jawa Barat 40132, Indonesia*

Agus Arsad − *UTM-MPRC Institute for Oil and Gas, Faculty of Chemical and Energy Engineering, Universiti Teknologi Malaysia, 81310 Skudai, Malaysia*

Wisup Bae − *Department of Energy and Mineral Resources Engineering, Sejong University, 05006 209 Seoul, Republic of Korea*

Ully Zakyatul Husna − *Pertamina Hulu Rokan, Sumatera Region Zone 3, Pekanbaru 28131, Indonesia*

Ai Ling Pang − *Department of Chemical Science, Faculty of Science, Universiti Tunku Abdul Rahman, 31900 Kampar, Malaysia*

Rifal Fauzi − *Department of Petroleum Engineering, Universitas Islam Riau, Riau 28284, Indonesia*

Complete contact information is available at: https://pubs.acs.org/10.1021/acsomega.2c08085

Notes

The authors declare no competing financial interest.

ACKNOWLEDGMENTS

This work is supported by Universitas Islam Riau (UIR) and Universiti Teknologi Malaysia (UTM) for the research grant (WCP Program 2021 SK no. 2817/E4.1/KK.04.0/2021 and UTM 4B549) and also supported by the Sejong University (Korea). The authors also wish to thank CMG for the encouragement of writing this paper.

ABBREVIATIONS

APE = acoustic pulse-echo

https://doi.org/10.1021/acsomega.2c08085
ACS Omega 2023, 8, 8703−8711

API = American Petroleum Institute
cm = centimeter
CO_2 = carbon dioxide
Cp = centipoise
EOR = enhanced oil recovery
EOS = observation and equation of state
H_2S = hydrogen sulfide
IFT = interfacial tension
MEA = monoethanol amine
mm = millimeter
MMP = minimum missible pressure
N_2 = nitrogen
°C = Celsius
Pb = bubble point pressure
Pr = reservoir pressure
psi = pounds per square inch
R^2 = correlation coefficients
RF = recovery factor
Tr = reservoir temperature
VIT = vanishing interfacial tension

■ REFERENCES

(1) Bao, B.; Feng, J.; Qiu, J.; Zhao, S. Direct Measurement of Minimum Miscibility Pressure of Decane and CO2 in Nanoconfined Channels. *ACS Omega* **2021**, *6* (1), 943−953.

(2) Czarnota, R.; Knapik, E.; Wojnarowski, P.; Janiga, D.; Stopa, J. Carbon Dioxide Separation Technologies. *Arch. Min. Sci.* **2019**, *64* (3), 487−498.

(3) Rachmat, S.; Pramana, A. A.; NW Ayu, L. F. Indonesia's Unconventional Resources, Modified Resource Triangle, and a Typical Example of Stimulation of Coalbed Methane Reservoir. *Mod. Appl. Sci.* **2012**, *6* (6), 99−111.

(4) Dong, M.; Huang, S.; Srivastava, R. Effect of Solution Gas in Oil on CO2 minimum Miscibility Pressure. *J. Can. Pet. Technol.* **2000**, *39* (11), DOI: 10.2118/00-11-05.

(5) Yellig, W. F.; Metcalfe, R. S. Determination and Prediction of CO2 minimum Miscibility Pressures (Includes Associated Paper 8876). *J. Pet. Technol.* **1980**, *32* (01), 160−168.

(6) Yu, H.; Lu, X.; Fu, W.; Wang, Y.; Xu, H.; Xie, Q.; Qu, X.; Lu, J. Determination of Minimum near Miscible Pressure Region during CO2 and Associated Gas Injection for Tight Oil Reservoir in Ordos Basin, China. *Fuel* **2020**, *263*, 116737.

(7) Zheng, L.; Ma, K.; Yuan, S.; Wang, F.; Dong, X.; Li, Y.; Du, D. WITHDRAWN: Determination of the Multiple-Contact Minimum Miscibility Pressure of CO2/Oil System Using Oil Droplet Volume Measurement Method. *J. Pet. Sci. Eng.* **2019**, 106578.

(8) Ahmad, W.; Vakili-Nezhaad, G.; Al-Bemani, A. S.; Al-Wahaibi, Y. Experimental Determination of Minimum Miscibility Pressure. *Procedia Eng.* **2016**, *148*, 1191−1198.

(9) Zhao, Y.; Fan, G.; Song, K.; Li, Y.; Chen, H.; Sun, H. The Experimental Research for Reducing the Minimum Miscibility Pressure of Carbon Dioxide Miscible Flooding. *Renew. Sustain. Energy Rev.* **2021**, *145*, 111091.

(10) Ahmed, T. Minimum Miscibility Pressure from EOS. Paper presented at the Canadian International Petroleum Conference, Calgary, Alberta, June 2000, paper PETSOC-2000-001, DOI: 10.2118/2000-001.

(11) Chen, H.; Li, B.; Duncan, I.; Elkhider, M.; Liu, X. Empirical Correlations for Prediction of Minimum Miscible Pressure and Near-Miscible Pressure Interval for Oil and CO2 Systems. *Fuel* **2020**, *278*, 118272.

(12) Soori, T.; Rassoulinejad-Mousavi, S. M.; Zhang, L.; Rokoni, A.; Sun, Y. A Machine Learning Approach for Estimating Surface Tension Based on Pendant Drop Images. *Fluid Phase Equilib.* **2021**, *538*, 113012.

(13) Chen, H.; Zhang, C.; Jia, N.; Duncan, I.; Yang, S.; Yang, Y. Z. A Machine Learning Model for Predicting the Minimum Miscibility Pressure of CO2 and Crude Oil System Based on a Support Vector Machine Algorithm Approach. *Fuel* **2021**, *290*, 120048.

(14) Nobakht, M.; Moghadam, S.; Gu, Y. Determination of CO2 minimum Miscibility Pressure from Measured and Predicted Equilibrium Interfacial Tensions. *Ind. Eng. Chem. Res.* **2008**, *47* (22), 8918−8925.

(15) Hemmati-Sarapardeh, A.; Ayatollahi, S.; Ghazanfari, M.-H.; Masihi, M. Experimental Determination of Interfacial Tension and Miscibility of the CO2-Crude Oil System; Temperature, Pressure, and Composition Effects. *J. Chem. Eng. Data* **2014**, *59* (1), 61−69.

(16) Yang, D.; Gu, Y. Interfacial Interactions Between Crude Oil and CO2 Under Reservoir Conditions. *Pet. Sci. Technol.* **2005**, *23* (9−10), 1099−1112.

(17) Abdurrahman, M.; Pramana, A. A.; Permadi, A. K.; Junin, R. *Fundamental of Minimum Miscibility Pressure Determination*; UIR Press: Pekanbaru, 2020.

(18) Adel, I. A.; Tovar, F. D.; Schechter, D. S. Fast-Slim Tube: A Reliable and Rapid Technique for the Laboratory Determination of MMP in CO_2 - Light Crude Oil Systems. Paper presented at the SPE Improved Oil Recovery Conference, Tulsa, Oklahoma, April 2016, paper SPE-179673-MS, DOI: 10.2118/179673-MS.

(19) Firoozabadi, A. *Thermodynamics of Hydrocarbon Reservoirs*, 1st ed.; McGraw Hill, 1999.

(20) Saad, S. M. I.; Policova, Z.; Neumann, A. W. Design and Accuracy of Pendant Drop Methods for Surface Tension Measurement. *Colloids Surfaces A Physicochem. Eng. Asp.* **2011**, *384* (1−3), 442−452.

(21) Almobarak, M.; Wu, Z.; Zhou, D.; Fan, K.; Liu, Y.; Xie, Q. A Review of Chemical-Assisted Minimum Miscibility Pressure Reduction in CO2 Injection for Enhanced Oil Recovery. *Petroleum* **2021**, *7* (3), 245−253.

(22) Jessen, K.; Orr, F. M. On Interfacial-Tension Measurements to Estimate Minimum Miscibility Pressures. *SPE Reserv. Eval. Eng.* **2008**, *11* (05), 933−939.

(23) Zhang, K.; Jia, N.; Zeng, F. Application of Predicted Bubble-Rising Velocities for Estimating the Minimum Miscibility Pressures of the Light Crude Oil-CO2 Systems with the Rising Bubble Apparatus. *Fuel* **2018**, *220*, 412−419.

(24) Yang, Z.; Liu, X.; Hua, Z.; Ling, Y.; Li, M.; Lin, M.; Dong, Z. Interfacial Tension of CO2 and Crude Oils under High Pressure and Temperature. *Colloids Surfaces A Physicochem. Eng. Asp.* **2015**, *482*, 611−616.

(25) Abdurrahman, M.; Permadi, A. K. Minimum Miscibility Pressure Estimation through Interfacial Tension Test Using Pendant Drop Method. *J. Teknol. Miny. dan Gas Bumi* **2019**, *11* (2), 111−118.

(26) Abdurrahman, M.; Bae, W.; Permadi, A. K. Determination and Evaluation of Minimum Miscibility Pressure Using Various Methods: Experimental, Visual Observation, and Simulation. *Oil Gas Sci. Technol.* **2019**, *74*, 55.

(27) Wang, H.; Torabi, F.; Zeng, F.; Xiao, H. Experimental and Numerical Study of Non-Equilibrium Dissolution and Exsolution Behavior of CO2 in a Heavy Oil System Utilizing Hele-Shaw-like Visual Cell. *Fuel* **2020**, *270*, 117501.

(28) Alhosani, A.; Lin, Q.; Scanziani, A.; Andrews, E.; Zhang, K.; Bijeljic, B.; Blunt, M. J. Pore-Scale Characterization of Carbon Dioxide Storage at Immiscible and near-Miscible Conditions in Altered-Wettability Reservoir Rocks. *Int. J. Greenh. Gas Control* **2021**, *105*, 103232.

(29) Lashkarbolooki, M.; Eftekhari, M. J.; Najimi, S.; Ayatollahi, S. Minimum Miscibility Pressure of CO2 and Crude Oil during CO2 Injection in the Reservoir. *J. Supercrit. Fluids* **2017**, *127*, 121−128.

(30) Zhao, H.; Song, C.; Zhang, H.; Di, C.; Tian, Z. Improved Fluid Characterization and Phase Behavior Approaches for Gas Flooding and Application on Tahe Light Crude Oil System. *J. Pet. Sci. Eng.* **2022**, *208*, 109653.

(31) Czarnota, R.; Janiga, D.; Stopa, J.; Wojnarowski, P. Acoustic Investigation of CO2Mass Transfer into Oil Phase for Vapor Extraction Process under Reservoir Conditions. *Int. J. Heat Mass Transfer* **2018**, *127*, 430−437.

https://doi.org/10.1021/acsomega.2c08085
ACS Omega 2023, 8, 8703−8711